AGU PUBLICATIONS

Global Biogeochemical Cycles

RESEARCH ARTICLE
10.1002/2015GB005205

Key Points:
- Significant seasonality found in NCP including fall and winter heterotrophy
- Elevated PIC:POC ratio relative to the global average
- Continuous in situ observations are required to develop a robust carbon cycle baseline

Supporting Information:
- Text S1, Figure S1, and Tables S1 and S2
- Text S2

Correspondence to:
A. J. Fassbender,
andrea.fassbender@noaa.gov

Citation:
Fassbender, A. J., C. L. Sabine, and M. F. Cronin (2016), Net community production and calcification from 7 years of NOAA Station Papa Mooring measurements, *Global Biogeochem. Cycles*, *30*, 250–267, doi:10.1002/2015GB005205.

Received 3 JUN 2015
Accepted 5 JAN 2016
Accepted article online 7 JAN 2016
Published online 20 FEB 2016

Net community production and calcification from 7 years of NOAA Station Papa Mooring measurements

Andrea J. Fassbender[1,2], Christopher L. Sabine[2], and Meghan F. Cronin[2]

[1]School of Oceanography, University of Washington, Seattle, Washington, USA, [2]NOAA Pacific Marine Environmental Laboratory, Seattle, Washington, USA

Abstract Seven years of near-continuous observations from the Ocean Station Papa (OSP) surface mooring were used to evaluate drivers of marine carbon cycling in the eastern subarctic Pacific. Processes contributing to mixed layer carbon inventory changes throughout each deployment year were quantitatively assessed using a time-dependent mass balance approach in which total alkalinity and dissolved inorganic carbon were used as tracers. By using two mixed layer carbon tracers, it was possible to isolate the influences of net community production (NCP) and calcification. Our results indicate that the annual NCP at OSP is 2 ± 1 mol C m^{-2} yr^{-1} and the annual calcification is 0.3 ± 0.3 mol C m^{-2} yr^{-1}. Piecing together evidence for potentially significant dissolved organic carbon cycling in this region, we estimate a particulate inorganic carbon to particulate organic carbon ratio between 0.15 and 0.25. This is at least double the global average, adding to the growing evidence that calcifying organisms play an important role in carbon export at this location. These results, coupled with significant seasonality in the NCP, suggest that carbon cycling near OSP may be more complex than previously thought and highlight the importance of continuous observations for robust assessments of biogeochemical cycling.

1. Introduction

The biological consumption and export of carbon from the ocean surface to the abyssal sediments, commonly referred to as the biological pump, is a major pathway for long-term carbon sequestration from the atmosphere [*Ciais et al.*, 2013]. Each year, approximately 11 Pg C is exported from the ocean surface to the interior as sinking organic and inorganic carbon particles are degraded in the water column, and 0.2 Pg C is delivered to the sediments through this biologically mediated carbon transport [*Ciais et al.*, 2013]. In addition to other physical processes, the biological pump gives rise to a vertical carbon gradient in the ocean and contributes to maintaining an ocean carbon content that is ~50 times higher than that of the atmosphere [*Rhein et al.*, 2013]. Changes in the functionality of the biological pump could influence the structure of this vertical gradient, affecting the efficiency of anthropogenic carbon dioxide (CO_2) uptake at the ocean surface through various feedback mechanisms over societally relevant timescales [*Passow and Carlson*, 2012; *Ciais et al.*, 2013]. These feedback mechanisms have been discussed in the literature but are not well understood due to complex ecosystem interactions and uncertain biogeochemical responses to anthropogenic ocean warming and acidification. In order to identify changes in the efficiency of the biological pump and quantitatively assess the climate implications of altered carbon cycling, a well constrained marine carbon cycle budget is needed.

Significant effort has been made to better understand marine carbon cycling. These efforts include observations from time series sites, such as Bermuda Atlantic Time-series Study (BATS) [*Bates*, 2012; *Lomas et al.*, 2013], European Station for Time series in the Ocean [*González-Dávila et al.*, 2010], Hawaii Ocean Time-series [*Winn et al.*, 1998; *Brix et al.*, 2004; *Dore et al.*, 2009], Ocean Station Papa (OSP) [*Wong et al.*, 2002c; *Timothy et al.*, 2013], and Carbon Retention in a Colored Ocean [*Taylor et al.*, 2012; *Astor et al.*, 2013]. Long-term observations from these stations integrate over natural oscillations and stochastic variability to reveal multidecadal trends as well as seasonal patterns of marine carbon cycling [*Bates et al.*, 2014]. Many of the longest and most robust observational time series come from ship based work where sites are sampled at least four times per year. At these sites, globally consistent trends are emerging with regard to surface ocean carbonate chemistry, showing that modern ocean CO_2 uptake and pH declines have been primarily controlled by CO_2 solubility [*Bates et al.*, 2014; *Lauvset et al.*, 2015]. There are, however, a few outliers, indicating that the carbonate chemistry changes in some regions may not be driven solely by the

atmospheric CO_2 increase and that physical and/or biogeochemical processes may be influencing surface ocean carbon dynamics in these locations [*Bates et al*., 2014].

Moorings have become useful tools for studying complex and episodic processes that require continuous observations to unravel. With the ability to resolve both long-term trends and intermittent events, moored time series observations can be used to learn about carbon cycling in remote locations and to develop modern, regional baselines for the biological pump [*McGillicuddy et al*., 1998, 2007; *Wong et al*., 1999; *Hamme et al*., 2010]. High temporal resolution CO_2 observations from moorings have proven extremely useful in identifying stochastic biological events that may have been misinterpreted in a lower frequency data set [*Hamme et al*., 2010]. This type of event-scale resolution is more important than ever when analyzing data sets for climate signals, which can be obscured by sample frequency biasing [*Bates et al*., 2014]. In addition to the immediate utility of using biogeochemical mooring data to study carbon cycling, these platforms are useful for calibrating sensors on autonomous floats and gliders and may assist the development and training of satellite products for carbon cycle research [*Gledhill et al*., 2009; *Johnson et al*., 2009; *Hales et al*., 2012].

Ocean Station Papa (OSP) is a time series site located at 50°N, 145°W in a region of high annual atmospheric CO_2 uptake in the subarctic northeast Pacific Ocean [*Takahashi et al*., 2009; *Ayers and Lozier*, 2012]. OSP began as a weather ship station in 1956. When the program concluded in 1981, the Canadian Department of Fisheries and Oceans Line P program continued to make repeat hydrographic cruises at least two to three times per year through the present date [*Freeland*, 2007]. From this rich hydrographic data set, net community production (NCP), defined as the gross photosynthetic production minus the community respiration in the surface mixed layer, has been estimated from ^{14}C bottle incubations [*Wong et al*., 1995], seasonal carbon and nutrient drawdown ratios [*Takahashi et al*., 1993; *Wong et al*., 2002a, 2002b], thorium and uranium isotopes [*Charette et al*., 1999], oxygen mass balances [*Emerson*, 1987; *Emerson et al*., 1991; *Emerson and Stump*, 2010; *Giesbrecht et al*., 2012; *Juranek et al*., 2012; *Lockwood*, 2013], and one-dimensional model simulations [*Signorini et al*., 2001; *Wong et al*., 2002c]. The total NCP over a given year, commonly referred to as the annual net community production (aNCP), is an upper limit on biologically mediated carbon export from the ocean surface to the interior each year, integrating both the particulate and the dissolved organic carbon production.

In June 2007, a NOAA surface mooring carrying physical and biogeochemical sensors was deployed at OSP beginning a high-frequency, in situ observational time series that continues to the present date. Oxygen and total gas pressure measurements from the 2007–2008 OSP mooring deployment were used to assess NCP [*Emerson and Stump*, 2010] and evaluate calcium carbonate ($CaCO_3$) production [*Emerson et al*., 2011]; however, estimates were confined to the summer due to complexities in using oxygen as a mixed layer tracer during winter. In order to estimate the aNCP, assumptions about the duration of the productive period as well as the consistency of the NCP rate throughout the year were required [*Emerson and Stump*, 2010]. With moored time series becoming a common component of long-term observing efforts, methods that can resolve the entire annual cycle of NCP in situ are needed to make use of these important and growing data sets [*Sutton et al*., 2014].

Here we evaluate seasonal and interannual variability in NCP and $CaCO_3$ production at OSP from 7 years of high-frequency moored observations using a dual tracer, mixed layer carbon budget. Changes in mixed layer dissolved inorganic carbon (DIC) and total alkalinity (TA) are used to diagnostically isolate physical, chemical, and biological carbon transformations and assess their annual contributions to surface ocean carbon inventory changes. The use of two mixed layer carbon tracers allows us to isolate organic carbon production (NCP) from inorganic carbon production ($CaCO_3$). This work contributes to the quantitative development of a modern baseline for carbon cycling in this important ocean carbon sink region [*Takahashi et al*., 2006, 2009; *Ayers and Lozier*, 2012].

2. Data

2.1. Mooring Data

The NOAA Station Papa mooring, deployed in June 2007 at 50°N, 145°W, contributes to the global network of OceanSITES time series reference stations [*Send et al*., 2010]. The mooring carries a suite of meteorological, physical, and biogeochemical sensors to monitor the air-sea exchanges of heat, moisture, momentum, and

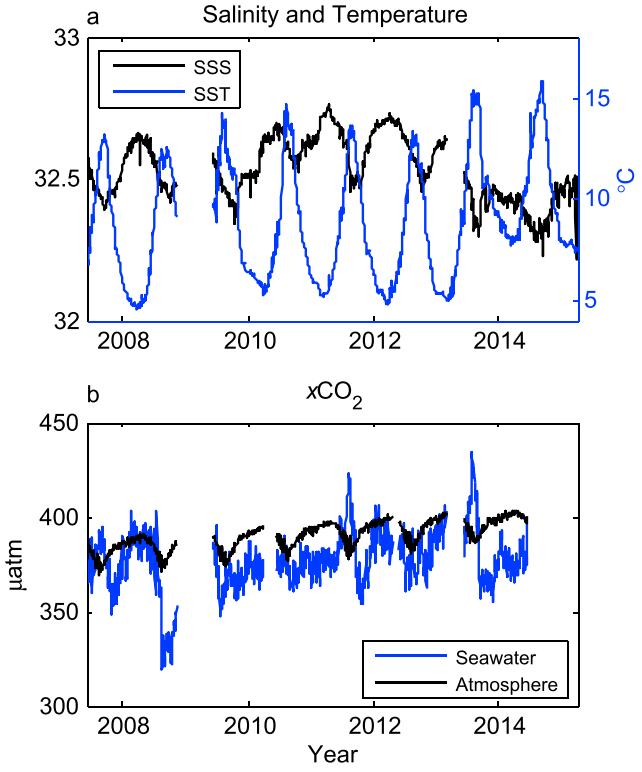

Figure 1. Time series of sea surface (a) salinity and temperature, and (b) seawater and atmospheric boundary layer xCO_2 at Ocean Station Papa.

carbon dioxide. It is also designed to monitor ocean acidification and upper ocean temperature, salinity, oxygen, and near surface currents. In particular, the buoy houses two inorganic carbon sensors used in this analysis: a Sunburst SAMI unit that measures sea surface pH and a Battelle Memorial Institute $MAPCO_2$ system that monitors the mole fraction of carbon dioxide (xCO_2) in seawater and in the atmospheric boundary layer. As discussed later in sections 3.1.1, 3.1.2, and 3.2, these measurements are used to calculate DIC and to estimate the air-sea CO_2 flux.

The analysis method described in the next section relies upon computing the sources and sinks of carbon within the mixed layer. Mixed layer depth, defined here as the depth where density increases by 0.03 kg m^{-3} from the 10 m density [*de Boyer Montégut et al.*, 2004], is determined using in situ measurements of salinity and temperature from sensors on the mooring line. Mixed layer velocity, used to estimate horizontal advection, is based upon current meter data from 5 m, 15 m, and 35 m, and a nearby upward looking Acoustic Doppler Current Profiler when available. Diffusivity at the base of the mixed layer was estimated by closing the mixed layer heat budget following *Cronin et al.* [2015]. The carbon budget, thus, relies upon nearly every measurement made on the mooring. These data and details about the specific sensors and their orientations during each deployment can be found on the Ocean Climate Stations web page (http://www.pmel.noaa.gov/OCS/Papa/).

Sensors on the mooring have operated almost continuously from 2007 to 2014 (Figure 1). The mooring and all sensors are recovered and a fresh system is redeployed every year, typically in June. In fall of 2008, the mooring broke free resulting in a large data gap from November 2008 to June 2009. Smaller periods of missing data in the xCO_2 time series (Figure 1b) were caused by sensor or battery failure. Due to the numerous sensors on the mooring, each programmed to sample at different frequencies, all data have been daily averaged and centered on 12:00 Greenwich Mean Time for this analysis.

2.2. Repeat Hydrography Data

Repeat hydrography cruise data that are publicly available from the Carbon Dioxide Information Analysis Center have been incorporated into the analysis for the development of relationships between carbonate system parameters (DIC and TA) and other commonly measured variables. Details about the use of these data are presented in sections 3.1.1 and 3.3. The specific cruise data used in this analysis include Climate Variability and Predictability (CLIVAR) Line P16 North in 2006 and in 2008, CLIVAR Line P01 in 2007, and Line P cruises between 1994 and 2010; applying Pacific Ocean Interior Carbon (PACIFICA) Database corrections when appropriate (Figure 2, http://cdiac.ornl.gov/oceans/PACIFICA/) [*Fukasawa et al.*, 2007; *Feely et al.*, 2008, 2011; *Miller et al.*, 2010]. In addition, 1° optimally interpolated data fields from the 2013 World Ocean Atlas (WOA) are used herein and discussed in section 3.3 [*Garcia et al.*, 2013a, 2013b; *Locarnini et al.*, 2013; *Zweng et al.*, 2013].

2.3. Satellite Data

There are very few time periods when xCO_2 measurements are available and other sensor data are not. A 2 week data gap in anemometer wind speed measurements in 2008 was filled using 0.25°, 6-hourly, cross-calibrated

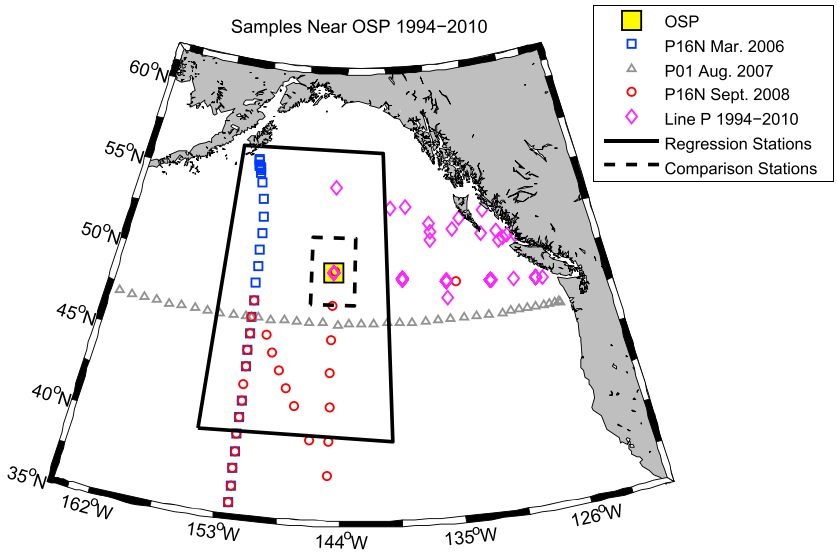

Figure 2. Map showing Ocean Station Papa (50°N, 145°W), nearby station locations from three CLIVAR repeat hydrography cruises between 2006 and 2008, and stations from numerous Line P cruises between 1994 and 2010. Months stated in the figure legend are when the cruises passed near Ocean Station Papa. The solid lined box includes stations used to develop a regional TA proxy. The dashed line box includes stations shown in Figure 4.

multiplatform ocean surface winds from NASA [*Atlas et al.*, 2011]. During periods when ADCP and current meter data are not available, 1/3°, 5 day resolution Ocean Surface Current Analysis – Realtime (OSCAR) satellite-based surface currents are used [*Bonjean and Lagerloef*, 2002]. Vertical velocity was estimated from the wind stress curl, assuming Ekman physics [*Cronin et al.*, 2013], using the daily Advanced Scatterometer wind stress data set [*Bentamy and Fillon*, 2012] and Archiving, Validation, and Interpretation of Satellite Oceanographic data absolute surface geostrophic velocities available from http://www.aviso.altimetry.fr.

3. Methods

Dissolved inorganic carbon (DIC) refers to the sum of the concentrations of carbonic acid (H_2CO_3), bicarbonate ion (HCO_3^-), carbonate ion (CO_3^{2-}), and CO_2 in aqueous solution:

$$\mathrm{DIC} = [CO_2] + [H_2CO_3] + [HCO_3^-] + [CO_3^{2-}] \quad (1)$$

DIC is influenced by all carbon transformations in the mixed layer including air-sea gas exchange (Gas), physical transport and mixing (Phys), concentration effects caused by evaporation and precipitation (EP), and the biological processes of organic (NCP) and inorganic ($CaCO_3$) carbon production:

$$\frac{\partial \mathrm{DIC}}{\partial t} = \left.\frac{\partial \mathrm{DIC}}{\partial t}\right|_{\mathrm{Gas}} + \left.\frac{\partial \mathrm{DIC}}{\partial t}\right|_{\mathrm{Phys}} + \left.\frac{\partial \mathrm{DIC}}{\partial t}\right|_{\mathrm{EP}} + \left.\frac{\partial \mathrm{DIC}}{\partial t}\right|_{\mathrm{NCP}} + \left.\frac{\partial \mathrm{DIC}}{\partial t}\right|_{\mathrm{CaCO_3}} \quad (2)$$

In situ observations from the NOAA Station Papa mooring can be used along with cruise data to estimate the term on the left-hand side and the first three terms on the right-hand side (i.e., Gas, Phys, and EP), leaving one equation and two unknowns. In order to close the budget, a second mixed layer tracer is required. Total alkalinity (TA) is the charge balance in seawater, defined as the excess of proton acceptors over proton donors [*Wolf-Gladrow et al.*, 2007]:

$$\mathrm{TA} = [HCO_3^-] + 2^*[CO_3^{2-}] + [B(OH)_4^-] + [HPO_4^{2-}] + 2^*[HPO_4^{3-}] \ldots + [OH^-] - [H^+] \quad (3)$$

TA is influenced by all of the same processes as DIC excluding gas exchange because dissolution of CO_2 has no net influence on the TA charge balance:

$$\frac{\partial \mathrm{TA}}{\partial t} = \left.\frac{\partial \mathrm{TA}}{\partial t}\right|_{\mathrm{Phys}} + \left.\frac{\partial \mathrm{TA}}{\partial t}\right|_{\mathrm{EP}} + \left.\frac{\partial \mathrm{TA}}{\partial t}\right|_{\mathrm{NCP}} + \left.\frac{\partial \mathrm{TA}}{\partial t}\right|_{\mathrm{CaCO_3}} \quad (4)$$

As with the DIC budget (2), the term on the left-hand side and the first two terms on the right-hand side of (4) can be estimated from in situ OSP mooring observations and cruise data. DIC and TA are stoichiometrically related during the biological processes of photosynthesis and respiration (NCP) as well as calcium carbonate dissolution and precipitation ($CaCO_3$). Thus, the time-dependent DIC and TA mass balances can be rearranged to give two equations and two unknowns, making it possible to close the mixed layer budgets.

Similar diagnostic carbon budget assessments have been made using ship-based data [*Gruber et al*., 1998; *Quay and Stutsman*, 2003; *Brix et al*., 2004; *Keeling et al*., 2004], and more recently using moored CO_2 time series [*Sugiura and Tsunogai*, 2005; *Chierici et al*., 2006; *Körtzinger et al*., 2008]. Although autonomous DIC and TA sensors are not currently commercially available for extended duration deployments on moorings, CO_2 measurements at numerous moored time series locations [*Sutton et al*., 2014] can be leveraged for more complex analyses and provide insights about biological carbon cycling until new sensors become available. Here we build off of the approaches of previous investigators and evaluate the drivers of seasonal and interannual DIC variability at Station Papa.

3.1. Creating a DIC Time Series

Evaluating changes in the carbon inventory of the surface mixed layer, and the processes responsible for those changes, requires a time series of DIC. Without direct observations of mixed layer DIC, alternative methods must be employed to reconstruct the carbon time series. Any two measurable carbonate system parameters (DIC, TA, xCO_2, pH) can be used to calculate all other parameters in the system; therefore, contemporaneous in situ measurements of pH and xCO_2 at OSP were used to estimate DIC and TA with the program CO_2sys [*van Heuven et al*., 2011] applying constants from *Lueker et al*. [2000] and *Dickson* [1990]. Comparison of the calculated DIC and TA concentrations with a limited number of high-quality discrete bottle samples collected near the mooring throughout the time series (Figure 2) revealed unrealistic excursions and biases in the calculated values (e.g., differences $>100\ \mu mol\ kg^{-1}$). These errors are the result of pH and/or xCO_2 measurement inaccuracies that are magnified in the calculations of other carbonate system parameters due to the strong covariance between the pH-xCO_2 pair. This concept has been well documented in the literature [*Dickson and Riley*, 1978; *Millero*, 2007] and has recently been revisited with regards to autonomous marine carbonate sensors [*Cullison Gray et al*., 2011; *Fassbender et al*., 2015]. Due to the challenges in using the pH-xCO_2 pair to calculated surface TA and DIC concentrations, an alternative method was developed.

3.1.1. Total Alkalinity Proxy

A surface ocean TA-salinity relationship was developed for the Alaska Gyre region using discrete samples collected during repeat hydrography cruises (Figure 2). Mean mixed layer salinity (PSS-78) and TA concentrations were regressed, yielding a statistically significant linear relationship ($TA = 37 \times salinity + 988$; $n = 68$) with an R^2 value of 0.74 (Figure 3). This regional regression was applied to in situ salinity measurements from the OSP time series to estimate sea surface TA for the 7 years of moored observations (Figure 4a). The 1σ calculation uncertainty, based on uncertainties in the regression and the discrete samples, is $\sim 3\ \mu mol\ kg^{-1}$. Discrete TA bottle samples collected in close proximity to the OSP mooring (Figure 2) between 2007 and 2012 show good agreement with the magnitude and seasonality of the predicted TA values. The mean difference between these bottle samples and the salinity-derived TA values is $0\ \mu mol\ kg^{-1}$, indicating that the broader, regional TA-salinity relationship holds well at OSP.

3.1.2. Calculating DIC

TA estimates were paired with in situ measurements of xCO_2 and pH to calculate two DIC time series using the program CO_2sys [*van Heuven et al*., 2011] applying constants from *Lueker et al*. [2000] and *Dickson* [1990] (Figure 4b). While both xCO_2 and pH perform well at predicting DIC when paired with TA, the xCO_2 time series has fewer data gaps and shows less sensor noise. In addition, discrete DIC bottle samples collected near OSP between 2007 and 2012 show better agreement with the DIC values computed from the TA-xCO_2 pair (mean difference of $2\ \mu mol\ kg^{-1}$). This agreement suggests that our TA proxy and DIC estimates are robust; therefore, DIC values derived from the TA-xCO_2 pair are used for the remainder of the analysis. The 1σ calculation uncertainty for DIC values derived from the TA-xCO_2 pair is $\sim 3\ \mu mol\ kg^{-1}$.

3.2. Gas Exchange

The daily air-sea CO_2 gas exchange was estimated from wind speed and the difference in CO_2 partial pressure (pCO_2) between the sea surface and atmosphere (ΔpCO_2):

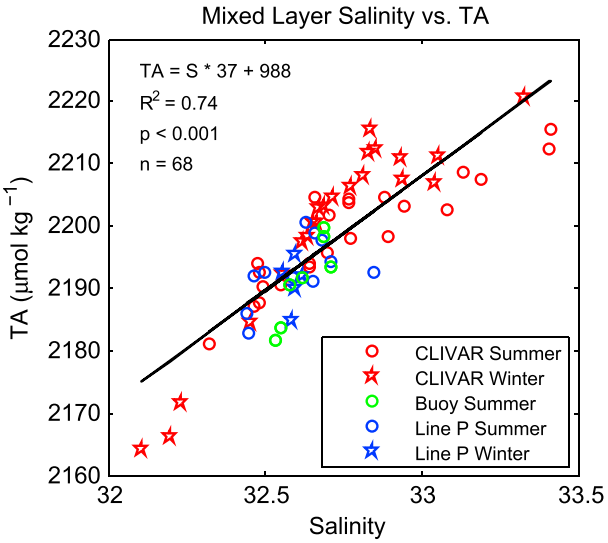

Figure 3. Mixed layer salinity versus total alkalinity relationship derived from samples collected inside the solid lined box in Figure 2. The symbols represent bottle sample data collected during CLIVAR and Line P cruises as well as next to the buoy during deployments. Winter refers to November–April.

$$\Delta pCO_2 = pCO_{2,\,sea} - pCO_{2,\,atm} \tag{5}$$

where pCO_2 is the product of total pressure and xCO_2. Winds measured at 4 m on the NOAA Station P buoy are converted to 10 m winds using the relationship of *Liu et al.* [1979] and are used to compute the CO_2 piston velocity (k) with the Schmidt number relationship of *Wanninkhof* [1992] and gas transfer parameterization of *Ho et al.* [2006]. The temperature and salinity dependent CO_2 solubility constant (K_H) of *Weiss* [1974] is used with the piston velocity (k) and ΔpCO_2 to compute daily air-sea CO_2 fluxes (mol CO_2 m^{-2} d^{-1}):

$$\left.\frac{\partial DIC}{\partial t}\right|_{Gas} = F = k \times K_H \times \Delta pCO_2 \tag{6}$$

The flux (F) is divided by mixed layer depth and density to convert to units of µmol DIC kg^{-1} d^{-1}.

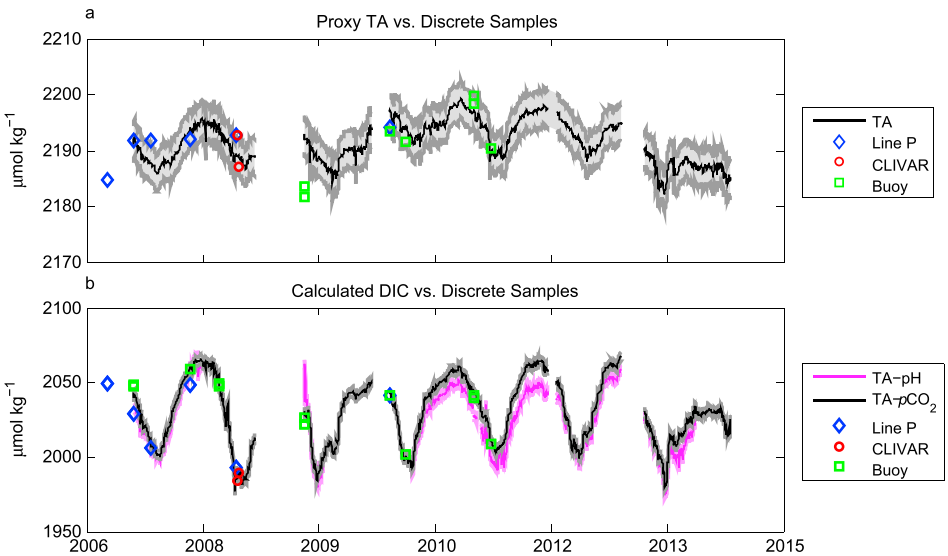

Figure 4. (a) TA estimated from the regional TA-salinity relationship and (b) DIC values computed from the TA-pH and TA-pCO_2 pairs using the program CO_2sys with error estimates shaded. Discrete TA and DIC bottle samples collected within the dashed black box region in Figure 2 between 2007 and 2012 are shown for comparison.

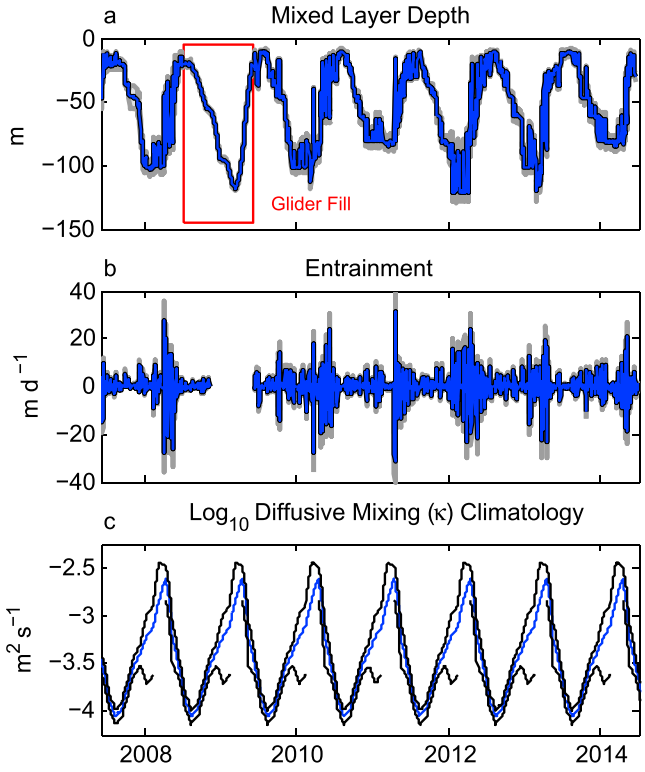

Figure 5. (a) Mixed layer depth and (b) entrainment time series with error estimates shaded in gray. The red box in (a) highlights glider mixed layer depth estimates. (c) Monthly climatology of diffusivity (κ) at the base of the mixed layer with error estimates. The mid-February to mid-April diffusivity is not statistically discernable from zero, so the lower bound error estimate is not plotted.

3.3. Physical Transport

Physical transport processes affecting the mixed layer DIC and TA mass balance include advection, entrainment (and detrainment), and diffusive mixing, expressed here in terms of DIC:

$$\left.\frac{\partial \mathrm{DIC}}{\partial t}\right|_{\mathrm{Phys}} = -\boldsymbol{u_a}\cdot\nabla \mathrm{DIC}_a - \left(w_{-h} + \frac{\partial h}{\partial t}\right)\frac{(\mathrm{DIC}_a - \mathrm{DIC}_{-h})}{h} - \frac{\kappa}{h}\left.\frac{\partial \mathrm{DIC}}{\partial z}\right|_{z=-h} \quad (7)$$

where ∇ is the vector differential (i.e., gradient) operator, $\boldsymbol{u_a}$ and DIC_a are the vertically averaged horizontal velocity and DIC concentration within the mixed layer, and h is the mixed layer depth (Figure 5a). Likewise, w_{-h}, DIC_{-h}, κ, and $\partial \mathrm{DIC}\,\partial z^{-1}$ are the vertical velocity, DIC concentration, diffusivity, and vertical concentration gradient, respectively, all evaluated at the base of the mixed layer ($z=-h$) as defined in section 2.1. Due to a break in the mooring line and consequent loss of subsurface conductivity-temperature-depth sensors in fall of 2008, mixed layer depths during this period were estimated from an autonomous profiling glider that repeated a butterfly pattern around the mooring every 2 weeks (Noel Pelland, personal communication, 2015; Figure 5a).

The first term on the right-hand side of equation (7) accounts for horizontal advection of DIC. The second term accounts for entrainment and detrainment vertical velocities (Figure 5b) acting on DIC gradients within the mixed layer and was set to zero on days when the mixed layer depth shoaled ($\partial h\,\partial t^{-1} < 0$) with the assumption that DIC_a and DIC_{-h} will be equal during shoaling events. It should be noted that if the upwelling velocity (w_{-h}) is equal and opposite sign of the mixed layer depth change ($\partial h\,\partial t^{-1}$), this term will be zero. Likewise, if the DIC concentration is vertically uniform from the surface through the base of the mixed layer, then this term would also be zero. The third term accounts for diffusive turbulent mixing at the base of the mixed layer. A monthly climatology of diffusivity coefficient (κ) (Figure 5c) was determined from the residual heat flux out the base of the mixed layer estimated from the mixed layer heat budget at Station Papa for June 2007 to June 2013 [*Cronin et al.*, 2015]. A diffusivity coefficient was calculated only during periods when the thermal stratification

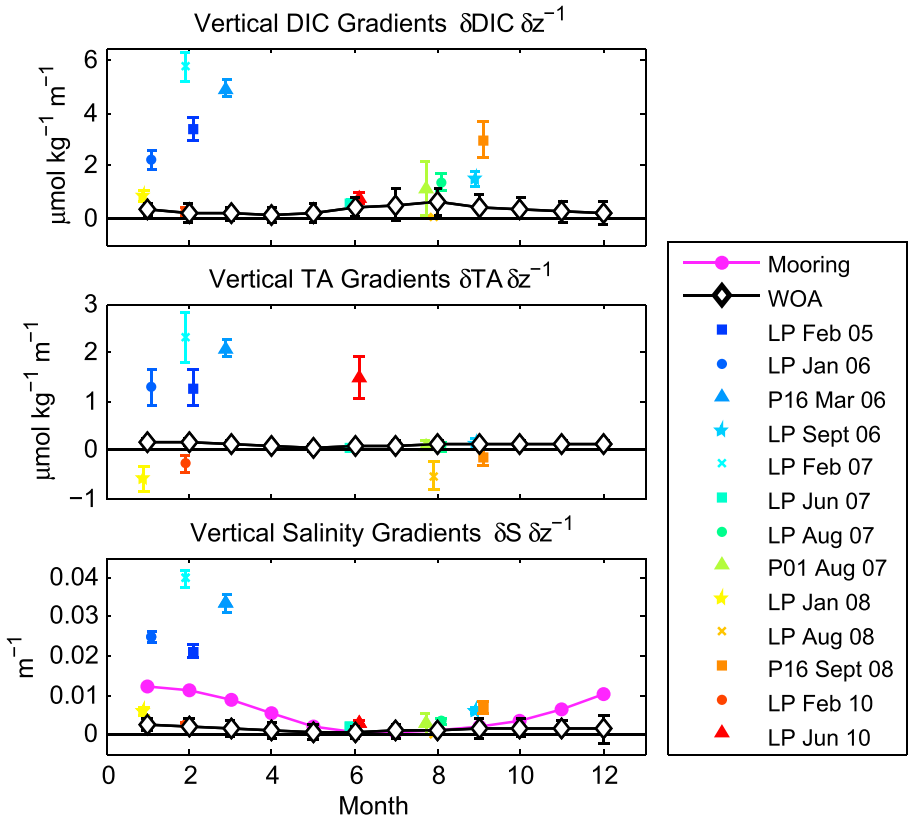

Figure 6. Monthly climatologies of vertical (a) DIC, (b) TA, and (c) salinity gradients at the base of the mixed layer derived from WOA and in situ, mooring data. Vertical gradients observed during three CLIVAR and 10 OSP cruises are shown for comparison. Values are slightly offset for easier viewing.

just below the mixed layer base was sufficiently strong and when the residual heat flux was down gradient. During late winter and early spring, the mixed layer was often shallower than the isothermal layer and acted as a "barrier layer" to diffusive mixing of heat. In these cases, κ often could not be estimated. Consequently, the late winter and early spring κ values have order 1 errors.

Continuous observations of horizontal and vertical DIC and TA gradients near OSP do not exist over the study period; however, high-quality carbon data have been collected near the mooring during repeat hydrography cruises that occurred just before or during the moored time series. Data from these cruises were used to construct multiple linear regression (MLR) relationships between DIC (and TA) and measured predictor variables in both the meridional and zonal directions. The meridional MLR was developed using data from the CLIVAR Line P16 North 2006 cruise, and the zonal MLR was developed using data from the CLIVAR Line P01 2007 cruise. Minimum latitude, longitude, and depth ranges included in the MLRs were determined from maximum monthly averaged horizontal and vertical flow velocities at OSP. For the meridional regressions, oxygen and temperature were the predictor variables for DIC and silicate was the predictor variable for TA. For the zonal regressions, phosphate was the predictor variable for DIC, and depth and silicate were the predictor variables for TA. MLR regression coefficients from the meridional and zonal fits were then applied to 2013 WOA monthly climatologies of the predictor variables to produce monthly DIC and TA fields. From these DIC and TA fields, vertically averaged mixed layer concentrations were determined at each 2013 WOA grid location and horizontal gradients were computed in the meridional and zonal directions. Vertical concentration gradients were calculated using the meridional TA and DIC fields, where $\delta X\,\delta z^{-1}$ in term three of (7) was evaluated as the last sample within the mixed layer subtracted from the first sample below the mixed layer and divided by their separation distance (Figure 6). These WOA derived gradient climatologies are used in (7) to estimate the physical transport budget terms of (2) and (4) on a monthly timescale.

To validate the WOA estimates, vertical gradients from three CLIVAR and 10 Line P cruises conducted between 2005 and 2010 are used for comparison, in addition to a vertical salinity gradient climatology estimated from subsurface sensors on the OSP mooring line (Figure 6). Gradient seasonalities agree well across estimates, but during the winter, there is more scatter in the cruise data and the in situ salinity estimates are larger than the WOA salinity gradients. This could mean that the WOA derived TA and DIC gradients are also underestimated during some months. To address the potential WOA gradient underestimation, in situ salinity gradients could be used for the budget analysis and, under the assumption that TA fluctuates conservatively with salinity at the base of the mixed layer, could be used to scale up the TA gradients. Unfortunately, DIC can vary significantly and independently of salinity, and it is not clear that DIC gradients are underestimated at the same time of year as the salinity gradients due to differences in the gradient seasonalities. As a result the WOA derived gradients are utilized herein, the implications and rational for which will be discussed more thoroughly in section 3.4.

3.4. Evaporation-Precipitation

The influence of evaporation and precipitation (EP) on mixed layer DIC and TA concentrations was determined using a mixed layer salinity mass balance, where changes in salinity over time are caused by physical transport processes within the water column and EP. Monthly climatologies of salinity from the 2013 WOA were used to determine vertical and horizontal salinity gradients (Figure 6c) and estimate the physical transport component of the salinity budget using (7). Subtracting this from the observed salinity changes leaves the EP term, evaluated on a monthly timescale.

$$\left.\frac{\partial \mathrm{Sal}}{\partial t}\right|_{\mathrm{EP}} = \frac{\partial \mathrm{Sal}}{\partial t} - \left.\frac{\partial \mathrm{Sal}}{\partial t}\right|_{\mathrm{Phys}} \tag{8}$$

The EP term is multiplied by the ratio of DIC to salinity (or TA to salinity) at the start of each deployment ($t = 1$) to scale to units of $\mu\mathrm{mol\,kg^{-1}\,d^{-1}}$:

$$\left.\frac{\partial \mathrm{DIC}}{\partial t}\right|_{\mathrm{EP}} = \left.\frac{\partial \mathrm{Sal}}{\partial t}\right|_{\mathrm{EP}} \times \left.\frac{DIC}{Sal}\right|_{t=1} \tag{9}$$

It should be noted that the TA to salinity ratio (~67 $\mu\mathrm{mol\,kg^{-1}}$) at the start of the deployment ($t = 1$) is not the slope of the regional TA-salinity regression (37 $\mu\mathrm{mol\,kg^{-1}}$; Figure 3). The regional salinity-TA regression slope includes the influence of EP, biology, and mixing processes. The TA to salinity ratio at the start of the deployment reflects the amount of TA and salt in the water at that time and is equal to the slope of the dilution line relative to that starting point, making it possible to isolate the fresh water influence (EP) on TA (and DIC).

EP estimates from a rain gauge on the mooring indicate that salinity should be reduced by an average of ~0.7 each year due to net precipitation. Evaluating budget equations (8) and (9) using the WOA vertical salinity gradients ($\delta S\,\delta z^{-1}$) gives a mean salinity decline of ~0.5, which is equivalent to a ~30% underestimation relative to the rain gauge data—likely due to underestimation of the physical input of salt. Evaluating the budget using in situ vertical salinity gradients from OSP gives a dilution that is 3 times too large (~2) relative to the rain gauge. Presuming that the in situ salinity gradients are correct (due to sensor redundancy and high sampling frequency) and the rain gauge data are reasonably accurate, these results suggest that the WOA salinity gradients may be too weak and the diffusive mixing term may be too large at some times. However, it is likely that the DIC budget has a similar bias of the same sign. As such, the primary benefit of using the WOA vertical salinity gradients to assess EP comes from the near cancelation of these physical budget term biases in the DIC mass balance. Substituting equations (8) and (9) into equation (2) and rearranging gives the following:

$$\frac{\partial \mathrm{DIC}}{\partial t} = \left.\frac{\partial \mathrm{DIC}}{\partial t}\right|_{\mathrm{Gas}} + \left.\frac{\partial \mathrm{DIC}}{\partial t}\right|_{\mathrm{Phys}} - \left(\left.\frac{\partial \mathrm{Sal}}{\partial t}\right|_{\mathrm{Phys}} \times \left.\frac{DIC}{Sal}\right|_{t=1}\right) + \left(\frac{\partial \mathrm{Sal}}{\partial t} \times \left.\frac{DIC}{Sal}\right|_{t=1}\right) + \left.\frac{\partial \mathrm{DIC}}{\partial t}\right|_{\mathrm{NCP}} + \left.\frac{\partial \mathrm{DIC}}{\partial t}\right|_{\mathrm{CaCO_3}} \tag{10}$$

Here the physical salinity budget term is scaled to DIC and subtracted from the physical DIC budget term, minimizing the impact of turbulent mixing errors and WOA gradient smoothing. While this convenient cancelation of biases minimizes errors in the overall DIC (and TA) budget, it is important to note that the individual EP and physical terms may be biased.

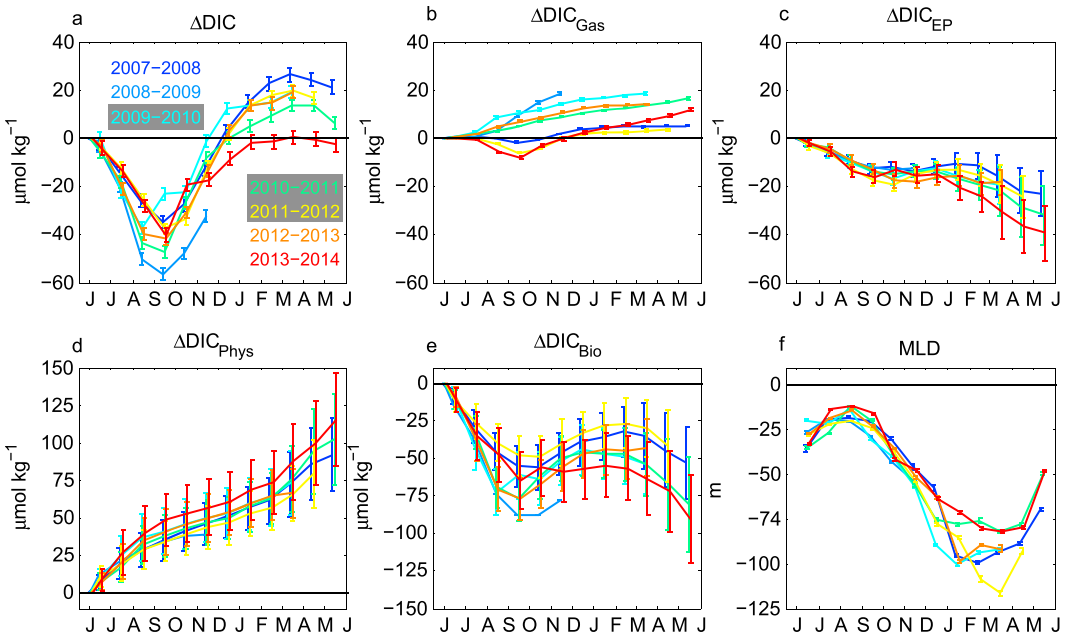

Figure 7. Results from the DIC budget analysis for each annual mooring deployment (colors) with error bars (not standard deviations). Average monthly (a) DIC concentration changes in the mixed layer relative to mid-June and the cumulative influences of (b) gas exchange, (c) EP, (d) physical transport, and (e) biological processes. (f) Mixed layer depth.

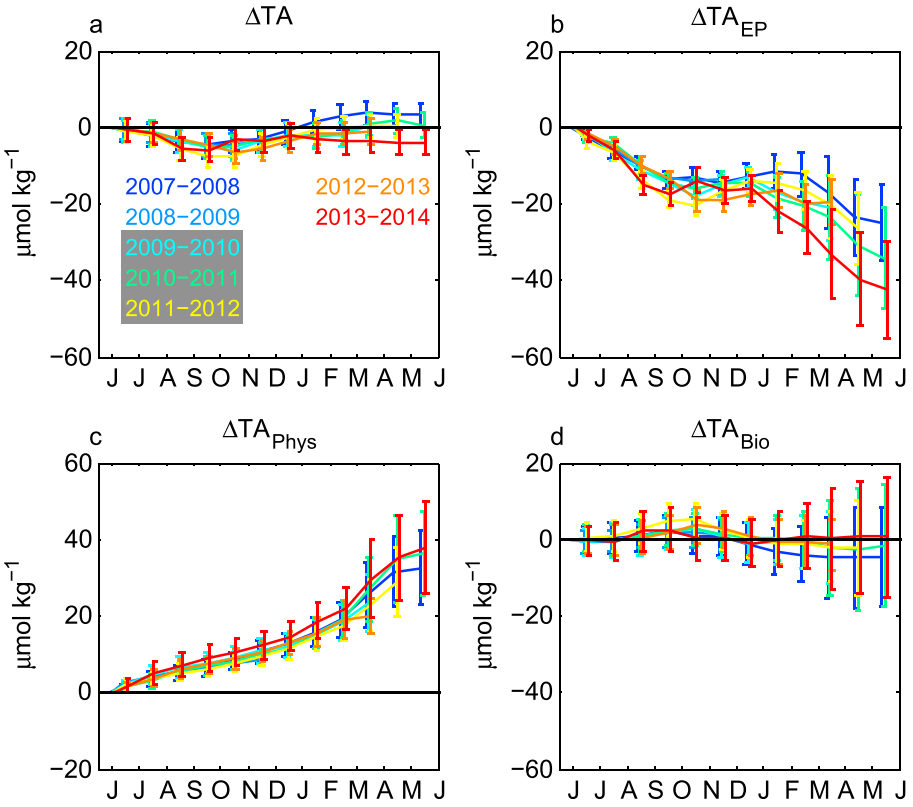

Figure 8. Results from the TA budget analysis for each annual mooring deployment (colors) with error bars (not standard deviations). Average monthly (a) TA concentration change in the mixed layer relative to mid-June and the cumulative influences of (b) EP, (c) physical transport, and (d) biological processes.

3.5. NCP and $CaCO_3$ Processes

With estimates of gas exchange, physical transport, and EP processes, this leaves only the biological terms (Bio), which can be estimated as a residual of the budget:

$$\left.\frac{\partial \mathrm{DIC}}{\partial t}\right|_{\mathrm{Bio}} = \left.\frac{\partial \mathrm{DIC}}{\partial t}\right|_{\mathrm{NCP}} + \left.\frac{\partial \mathrm{DIC}}{\partial t}\right|_{\mathrm{CaCO_3}} \tag{11}$$

$$\left.\frac{\partial \mathrm{TA}}{\partial t}\right|_{\mathrm{Bio}} = \left.\frac{\partial \mathrm{TA}}{\partial t}\right|_{\mathrm{NCP}} + \left.\frac{\partial \mathrm{TA}}{\partial t}\right|_{\mathrm{CaCO_3}} \tag{12}$$

NCP and $CaCO_3$ processes influence DIC and TA at well-known stoichiometric ratios. Production of 1 mol of $CaCO_3$ decreases the DIC concentration by 1 mol and the TA concentration by 2 mol. Similarly, organic matter production results in the consumption of 1 mol of phosphate (HPO_4^{2-}), 18 mol of H^+, and 117 mol of CO_2, causing TA to increase by 17 mol [*Anderson and Sarmiento*, 1994]. Therefore, the change in TA from organic matter production is equal to −17/117 times the change in DIC from organic matter production. These relationships make it possible to rearrange equations (11) and (12) to get two equations and two unknowns (not shown) and, thus, close the budget:

$$\left.\frac{\partial \mathrm{DIC}}{\partial t}\right|_{\mathrm{NCP}} = \frac{\left(\left.\frac{\partial \mathrm{TA}}{\partial t}\right|_{\mathrm{Bio}} - 2\times \left.\frac{\partial \mathrm{DIC}}{\partial t}\right|_{\mathrm{Bio}}\right)}{\left(-2 + \frac{-17}{117}\right)} \tag{13}$$

It should be noted that the residual includes the accumulation of all errors in the budget; therefore, a careful accounting of errors is performed. Manufacturer stated instrument errors were propagated through each of the calculations in this analysis using standard techniques. When computations were nonlinear or complex, a Monte Carlo approach was used in which 1000 iterations of the computation were conducted while varying input parameters around their errors in a Gaussian manner (~3σ). The standard deviation (σ) of the 1000 resultant values was then used as the error estimate for that parameter and was propagated through subsequent computations. Details about the error analysis, including information for variables that required data filling or more intensive error assessments, are described in the supporting information.

Parameterization of physical transport processes contributes most to uncertainties in the overall closing of the budget. Specifically, uncertainty in the vertical salinity, DIC, and TA gradients at the base of the mixed layer (~40–100%; Figures 6) coupled with uncertainties in the turbulent diffusion (κ; ~16–100%), give rise to the error bars shown in Figures 7 and 8, which contribute significantly to uncertainty in the annual estimates of DIC_{bio} and TA_{bio} and thus NCP and $CaCO_3$. While our error accounting is rigorous, the use of climatological κ values and concentration gradients means that interannual variability in the physical budget term is not resolved. Because the vertical diffusion term dominates the overall budget, interannual variations in NCP and $CaCO_3$ are also indiscernible, though seasonality can be evaluated.

4. Results

4.1. Mixed Layer Budget Evaluations

The NOAA Station Papa Mooring is replaced in mid-June of each year, making 19 June a logical start date ($t = 1$) for the annual mixed layer budget evaluations. Changes in mixed layer DIC and TA concentrations with time were computed by simply subtracting the concentration on 19 June from each daily value in the annual deployment, giving the total change at each time step in units of $\mu mol\,kg^{-1}$. Each of the other mixed layer budget terms, excluding gas exchange, was computed on a monthly time step in units of $\mu mol\,kg^{-1}\,mo^{-1}$; therefore, the daily estimates were binned and averaged by month for each deployment. Each budget term was then integrated in time through the duration of data collection in the respective year, giving a time series of cumulative mixed layer DIC and TA changes for each process contribution in units of $\mu mol\,kg^{-1}$ (Figures 7a and 8a). The following text in sections 4.1 and 4.2 includes mean values and standard deviations (1σ); however, error bars shown in Figures 7–9 are derived from propagated errors, not standard deviations, and reflect the uncertainty in our estimates.

Mixed layer DIC and TA show a regular seasonal cycle of decreasing concentrations in spring and summer followed by increasing concentrations in fall and winter. The average peak-to-peak amplitude of the seasonal DIC cycle (~56 ± 7 $\mu mol\,kg^{-1}$; 1σ given in text and errors shown in figures) is about 8 times larger than that of

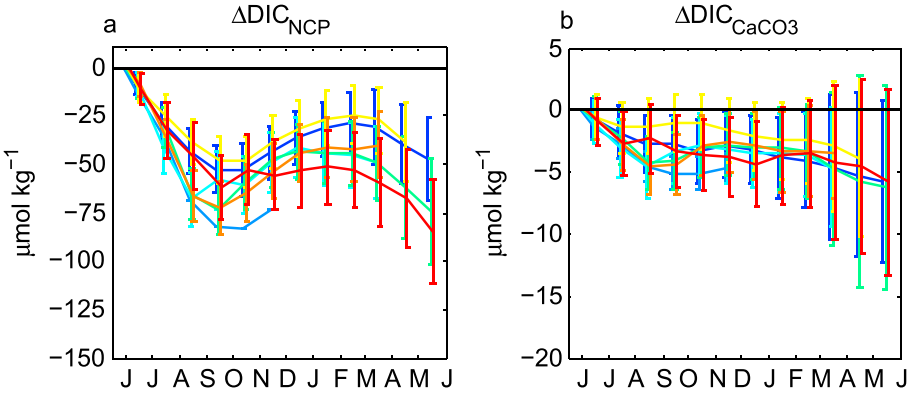

Figure 9. The cumulative influence of (a) NCP and (b) $CaCO_3$ process on the mixed layer DIC concentrations, with error bars (not standard deviations).

TA (~7 ± 1 μmol kg^{-1}) and agrees with prior observations in the subarctic current system and Alaska Gyre [*Wong et al*., 2002b]. The gas exchange contribution to mixed layer DIC changes is variable for each year, with all years showing a net invasion of CO_2 from the atmosphere and thus a net source of DIC to the mixed layer (~11 ± 6 μmol kg^{-1}; Figure 7b). The mean annual CO_2 flux into the ocean at OSP is 0.8 mol C m^{-2} yr^{-1} with a standard deviation of 0.4 mol C m^{-2} yr^{-1}, which is similar to the climatological mean annual CO_2 flux of ~1.25 mol C m^{-2} yr^{-1} estimated by *Takahashi et al*. [2009] for the year 2000. EP influences over the annual cycle act to dilute the DIC (~−31 ± 8 μmol kg^{-1}) and TA (~−34 ± 9 μmol kg^{-1}) concentrations due to net precipitation in this region (Figures 7c and 8b). Shallow mixed layer depths (Figure 7f) during summer and spring lead to maximum dilution for both parameters during these seasons. Physical processes exert the dominant control on the DIC concentration, adding a significant amount of carbon to the mixed layer throughout the year (~104 ± 13 μmol kg^{-1}), primarily through diffusive mixing (~90%) and diapycnal entrainment (~10%) as horizontal advection is found to be negligible (Figure 8c). For the TA budget, physical processes (~35 ± 3 μmol kg^{-1}) have a similar magnitude effect as the EP term, with diffusive mixing dominating the physical term (~90%) and entrainment (~10%) comprising the rest (Figure 8c).

Summing the contributions of gas exchange, evaporation-precipitation, and physical transport processes and subtracting them from the total changes in DIC and TA give the residual biological component of the budgets (Figures 7e and 8d). Biological processes remove DIC from the mixed layer over the course of the year, reducing the DIC concentration by ~75 ± 20 μmol kg^{-1}, which offsets much of the physical DIC input. Similarly, TA concentrations decline due to biological processes throughout the year but at a much lower level (~−2 ± 3 μmol kg^{-1}).

4.2. NCP and $CaCO_3$

The biological DIC term was decomposed into NCP and $CaCO_3$ processes using equation (13) to close the budget and equation (11) to solve for DIC_{CaCO3} (Figure 9). The results indicate that there is seasonality in the influence of organic carbon production on the mixed layer DIC concentration. NCP causes mixed layer DIC concentrations to decline in the spring and summer and to increase in fall and winter, though uncertainties are large. Observations over an entire annual cycle were captured during the 2007–2008, 2010–2011, and 2013–2014 mooring deployments. During these three sampling periods, the annual net community production (aNCP) reduced mixed layer DIC concentrations by an average of 69 ± 20 μmol DIC kg^{-1}. The influence of $CaCO_3$ production on the mixed layer DIC concentration is much smaller than NCP and does not show a clear seasonal cycle. During the three full-year mooring deployments, $CaCO_3$ production reduced mixed layer DIC concentrations by 6 ± 1 μmol DIC kg^{-1}.

4.3. Rates

Directly interpreting the DIC_{NCP} and DIC_{CaCO3} terms in units of concentration (μmol kg^{-1}) is not straight forward due to variability in the mixed layer depth throughout the year. To address this, the DIC_{NCP} and DIC_{CaCO3} terms were converted to monthly NCP and $CaCO_3$ rates (mmol C m^{-2} d^{-1}; Figures 10a and 10b). Positive NCP rates reflect net biological DIC consumption (autotrophy) and negative values reflect net biological DIC

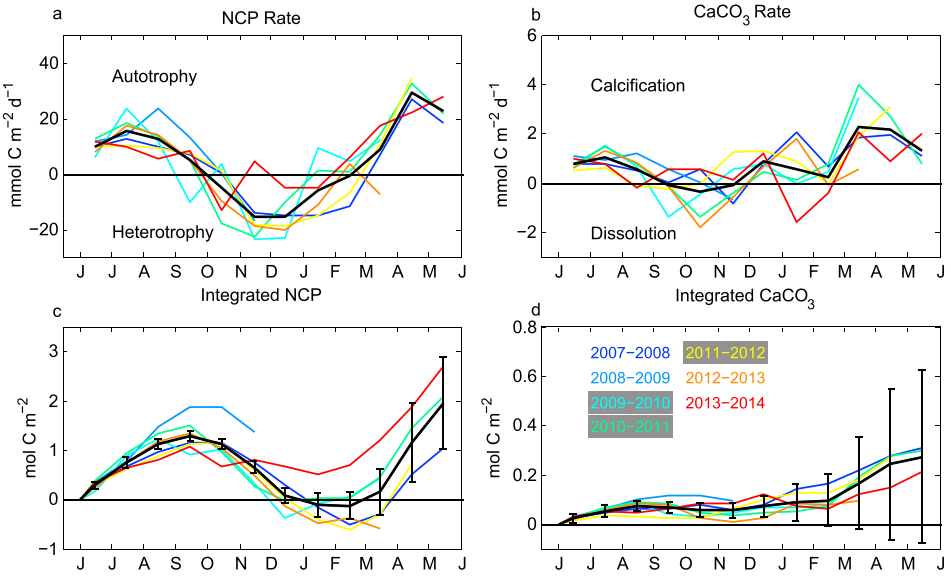

Figure 10. (a) NCP and (b) $CaCO_3$ rates as well as integrated (c) NCP and (d) $CaCO_3$ estimates from each deployment. Black lines show the mean of all years. Error bars are included for integrated NCP and $CaCO_3$ (not standard deviations).

production (heterotrophy). Positive $CaCO_3$ production rates reflect net calcification while negative values indicate net dissolution. Integrating the daily rates gives the cumulative column inventory of NCP and $CaCO_3$ (mol C m^{-2}) shown in Figures 10c and 10d. Annual mean composites are shown with black lines in Figures 10a–10d.

The results indicate that OSP is a region of net annual autotrophy and calcification, as found by numerous prior investigators [*Wong et al.*, 2002c; *Lipsen et al.*, 2007; *Emerson and Stump*, 2010; *Emerson et al.*, 2011]. Autotrophic NCP rates begin around March and peak in April, with sustained production through September. After September, heterotrophy is observed until January of the subsequent year. $CaCO_3$ production is sustained through most of the year, with peak calcification rates in March and April and the lowest rates found in and the fall. Cumulative summertime NCP results in ~1 mol C m^{-2} of production in the mixed layer from June to September (based on the composite), but this production is erased by the start of winter due to net respiration in the water column. Autotrophy resumes in spring, resulting in a mean mixed layer aNCP of 2 mol C m^{-2} yr^{-1} with an uncertainty of 1 mol C m^{-2} yr^{-1} (Table 1). The mean annual $CaCO_3$ production is 0.3 mol C m^{-2} yr^{-1} with an uncertainty of 0.3 mol C m^{-2} yr^{-1}.

Table 1. Summer and Annual Mixed Layer NCP Rates and aNCP Estimates at Ocean Station Papa

Method	Summer NCP Rate (mmol C m^{-2} d^{-1})	aNCP Rate (mmol C m^{-2} d^{-1})	aNCP (mol C m^{-2} yr^{-1})	Reference
NO_3^- drawdown	11.8			*Wong et al.* [2002c]
^{234}Th-^{238}U disequilibrium	8.1–9			*Charette et al.* [1999]
O_2 mass balance	8.3–25			*Emerson* [1987]
O_2, Ar, N_2 mass balance	8.9–11.7			*Emerson et al.* [1991]
In situ O_2, N_2	16.6		2.5 ± 1[a]	*Emerson and Stump* [2010]
O_2, Ar mass balance	13.1			*Giesbrecht et al.* [2012]
O_2, Ar mass balance	11.2[b]			*Juranek et al.* [2012]
DIC, TA mass balance	13 ± 5[c]	5 ± 2[d]	2 ± 1[e]	This study
Mean ± SD	12 ± 5	5	2.3 ± 0.4	

[a]Summertime NCP rate scaled for 150 days of fixed rate production ± error estimate.
[b]Mean of spring and summer oxygen production rates scaled using the 1.45 O_2/C conversion.
[c]Mean of June–August NCP rates from all years ± the standard deviation.
[d]Mean of aNCP estimates for 2007–2008, 2010–2011, and 2013–2014 divided by 365 ± the standard deviation.
[e]Mean of aNCP estimates for 2007–2008, 2010–2011, and 2013–2014 ± error estimate.

5. Discussion

Seven years of high-frequency CO_2 observations were used to compute net community production and calcification at Ocean Station Papa. Biological carbon consumption at this location largely compensates for vertical mixing processes that add DIC to the mixed layer throughout the year. NCP dominates the biological component of the mixed layer DIC drawdown with $CaCO_3$ production representing a small fraction of the annual productivity (Figures 9a and 9b).

The seasonal cycle of NCP rates (Figure 10a) at OSP indicates that the peak biological activity occurs in spring of each year and persists at a lower rate through summer. This finding differs from prior investigations that have found low variation in primary production between spring and summer [*Wong et al*., 1995]; however, sustained in situ observations of the productive period were lacking prior to the OSP mooring deployment. During spring, thermal stratification coupled with the passing of storms results in rapid changes in mixed layer depth at OSP (Figure 7f). The use of climatological vertical carbon gradients in our budget at times when the mixed layer is rapidly oscillating between depth levels but when net shoaling is occurring may result in overestimation of the vertical carbon input during intermittent deepening events. This would cause our spring estimates to be biased toward more NCP, which may explain the larger rates seen in these months. On the other hand, primary production in a shoaling mixed layer would increase the vertical carbon gradient at the base of the mixed layer, which could lead to an underestimation of the vertical carbon input and, thus, NCP during spring. In addition, the loss of NCP below the rapidly shoaling spring mixed layer would also lead to an underestimation of spring NCP, as discussed by *Körtzinger et al*. [2008]. Without in situ observations of the vertical carbon gradients it is challenging to determine how the use of climatological gradients may influence the spring NCP estimates; though gradients are at minimum during this season (Figure 6).

In October, NCP rates switch from being autotrophic to heterotrophic, indicating that community respiration is larger than the gross photosynthetic production in fall and winter. This seasonal heterotrophy has been identified once previously in the Alaska Gyre region by *Chierici et al*. [2006] using a mixed layer CO_2 budget approach based on ~ monthly observations throughout the year 2000. Sediment trap observations spanning more than two decades suggest that particle export at OSP occurs throughout the year, with peaks in the spring and summer months [*Wong et al*., 1999; *Timothy et al*., 2013]. In order to have a POC flux in fall and winter but still observe heterotrophic NCP rates, the remineralization of POC and DOC in the mixed layer must exceed the POC production rate. Spring and summer NCP at OSP sum to three times the winter carbon requirement for heterotrophy (~3 mol C m^{-2} versus ~1 mol C m^{-2}, respectively), which means that fall and winter heterotrophy could be fueled by local sources of carbon. Because there is continuous particle export during fall and winter [*Timothy et al*., 2013], it is likely that seasonal heterotrophy is primarily fueled by DOC rather than POC, as has been observed previously at BATS [*Carlson et al*., 1994].

In order to account for 1 mol C m^{-2} of seasonal heterotrophy in a ~75 m fall mixed layer, ~13 μmol kg^{-1} of DOC would need to be consumed. The mixed layer DOC concentration at OSP was ~55 μmol kg^{-1} in March 2006 during the CLIVAR P16 cruise, and *Wong et al*. [2002c] observed a similar DOC concentration (~65 μmol kg^{-1}) during February 1997, which increased to ~80 μmol kg^{-1} in June 1997 and was found to be as high as ~90 μmol kg^{-1} in May 1995. Deepening of a 25 m summer mixed layer with a DOC concentration of ~90 μmol kg^{-1} to a ~100 m winter mixed layer, given a subsurface (25 to 100 m) DOC concentration of ~50 μmol kg^{-1}, would result in a water column DOC concentration of 60 μmol kg^{-1}. Thus, most of the observed seasonal changes in DOC concentration can be explained by dilution [e.g., *Hansell*, 2001]; however, assuming that DOC is not building up at OSP, an additional 10 μmol kg^{-1} must be removed through further dilution or heterotrophy to get back to initial subsurface DOC value of ~50 μmol kg^{-1}. This additional 10 μmol kg^{-1} reduction of DOC agrees well with the requirement of ~13 μmol kg^{-1} needed to fuel the heterotrophic signal found herein. It should be noted, however, that a heterotrophic signal could also result from the underestimation of κ and/or the vertical carbon gradients at this time of year; therefore, further observations are needed to confirm the heterotrophic signal at OSP.

Prior investigators estimate that annual DOC production at OSP represents 25–50% of the primary production [*Bishop et al*., 1999], though there is some discrepancy among studies [*Wong et al*., 2002c]. In 2014, using apparent oxygen utilization (AOU) and DOC data from CLIVAR P16 near OSP, *Emerson* [2014] found that ~20% of the organic carbon remineralization in the upper pycnocline is caused by DOC degradation. Scaling the DOC:AOU ratio of 0.2 by the Redfield oxygen to carbon relationship of 1.45 [*Anderson and Sarmiento*, 1994]

Table 2. Ocean Station Papa and Global Ocean PIC:POC Ratio Estimates

	PIC:POC	Reference
OSP Estimate Method		
200 m sediment traps (1982–1993)	0.5	*Wong et al.* [1999]
50 m sediment traps (1987–1997)	0.4	*Wong et al.* [2002c]
^{14}C incubations (1998–2000)	0.25	*Lipsen et al.* [2007]
In situ O_2-, N_2-, pH- and pCO_2-based model (2007)	0.5	*Emerson et al.* [2011]
50 m sediment-trap-based estimate (1982–2006)	0.18	*Timothy et al.* [2013]
DIC, TA mass balance[a]	0.15–0.25	This study
Mean ± SD	0.3 ± 0.1	
Global Estimate Method		
Ocean general circulation model	0.09	*Jin et al.* [2006]
Ocean biogeochemical–transport box model	0.06 ± 0.03[b]	*Sarmiento et al.* [2002]
Mean ± SD	0.075 ± 0.02	

[a]Mean of 2007–2008, 2010–2011, and 2013–2014 deployments assuming 0% and 40% of aNCP is due to the export of DOC.
[b]Error estimate.

gives a DOC remineralization to DIC production ratio of ~0.3 in the upper pycnocline. Assuming this holds for all respiration occurring between the base of the seasonal mixed layer and pycnocline and given that the annual physical DIC input to the mixed layer, primarily though vertical processes, is ~100 μmol kg^{-1}, the annual physical DOC export would be ~30 μmol kg^{-1}. Thus, the physical export of DOC could account for up to 40% of the mixed layer DIC reduction attributed to NCP (~70 μmol kg^{-1}) in this region. These findings indicate that DOC transformation near OSP may play a more substantial role in carbon cycling than previously thought; contributing to seasonality in NCP and to the overall carbon export.

Seasonality in NCP indicates that estimates of aNCP based on discrete or single season rate evaluations may be biased unless the observations happen to reflect the mean annual NCP rate. In this analysis, the full annual cycle of NCP was resolved for three of the OSP mooring deployments, capturing spring and summer production as well as fall and winter heterotrophy. Most prior NCP estimates have been conducted during the summer period and agree well with our summer NCP rates (Table 1). In particular, *Emerson and Stump* [2010] used in situ oxygen data from the 2007–2008 OSP mooring deployment to estimate the summer NCP using a mass balance approach. They then scaled the summertime rate by 150 days (5 months) of production to estimate the aNCP, getting a value of 2.5 ± 1 mol C m^{-2} yr^{-1} (Table 1). Based on the analysis herein, there are approximately 7 months of productivity at OSP (~210 days). Scaling the mean summer NCP rate from *Emerson and Stump* [2010] by 210 days of production gives an aNCP estimate of 3.4 mol C m^{-2}, which is near our estimate of the total combined spring and summer production (~3 mol C m^{-2}), but exceeds the annual NCP estimate of 2 mol C m^{-2} by neglecting the heterotrophic season. These findings highlight the importance of resolving the full annual cycle of NCP for resolving biological processes near OSP.

$CaCO_3$ production at OSP begins in winter and peaks in spring, with sustained, lower production in summer. A few of the fall $CaCO_3$ production estimates suggest that dissolution is occurring, which is unexpected in this region where both aragonite and calcite are saturated at the sea surface [*Feely et al.*, 2002]. These values are not statistically significant but suggest that $CaCO_3$ production may be very low at this time of year. As previously discussed, 40% of the aNCP may be attributable to DOC export. As a result the PIC:POC ratio could range from 0.15 to 0.25, presuming that DOC export contributes to 0% to 40% of the aNCP, respectively. Prior PIC:POC estimates at OSP based on independent methodologies have found PIC:POC ratios ranging from 0.18 to 0.5 (Table 2), with estimates of the global average PIC:POC ratio near ~0.075 [*Sarmiento et al.*, 2002; *Jin et al.*, 2006; Table 2]. Thus, our findings add to the growing body of evidence that the eastern subarctic Pacific exhibits exceptionally high $CaCO_3$ production [*Wong et al.*, 1999, 2002c; *Lipsen et al.*, 2007; *Emerson et al.*, 2011; *Timothy et al.*, 2013].

6. Conclusions

Net community production (NCP) and calcium carbonate ($CaCO_3$) precipitation were estimated from 7 years of high-frequency moored observations at Ocean Station Papa (OSP). Surface ocean total alkalinity and dissolved inorganic carbon time series were derived from in situ observations of salinity and carbon dioxide

and used to diagnostically assess the influence of gas exchange, physical transport processes, evaporation and precipitation, NCP, and $CaCO_3$ production on mixed layer carbon inventories using a dual tracer mixed layer mass balance approach. Our results indicate that the average mixed layer aNCP at OSP is ~2 mol C m^{-2} yr^{-1} with an uncertainty of 1 mol C m^{-2} yr^{-1} and the average $aCaCO_3$ production is ~0.3 mol C m^{-2} yr^{-1} with an uncertainty of 0.3 mol C m^{-2} yr^{-1}. Significant seasonality in NCP, including seasonal heterotrophy, in this region where chlorophyll levels remain low year round and the system is known to be iron limited [*Martin and Fitzwater*, 1988], suggests that carbon cycling at OSP may be more complex than previously thought. Thus, discrete observations or single season assessments of NCP may not be robustly scalable to annual estimates of NCP, and PIC:POC estimates derived from chemical mass balances may need revisiting in light of potentially significant DOC cycling in this region. With a modern baseline for biological carbon cycling coming into focus at this location, continued observations will make it possible to evaluate how the biological pump is responding to ocean acidification and climate change.

Our methodology relies on salinity based estimates of surface ocean TA, which integrates the influence of $CaCO_3$ processes rather than independently resolving calcification in real time. While this adds uncertainty to the TA budget, uncertainty in the DIC budget is likely minimal due to the very close agreement between our estimated DIC time series and contemporaneous discrete bottle samples from the region. The TA budget could be improved with the aid of additional sensors that capture in situ calcification events. The pH and CO_2 sensors used during OSP deployments between 2007 and 2014 did not perform at the accuracy level required to calculate DIC and TA with confidence; however, these data have been used successfully to constrain carbonate system processes indirectly at OSP [*Emerson et al.*, 2011]. As autonomous DIC and TA sensors come online for moored application, direct observations of episodic $CaCO_3$ processes [*Wong et al.*, 1999] will improve our estimates. Until that time, the method used herein introduces an independent estimate of carbon cycling that adds to the growing body of work at OSP.

Acknowledgments
The authors thank Noel Pelland for providing glider data used in this analysis as well as Steven Emerson, Paul Quay, Seth Bushinsky, and two anonymous reviewers for their constructive feedback, which improved the manuscript. All mooring operations were performed aboard the CCGS Tully. We are grateful for the shiptime provided by the Line P program and efforts of the Captain, crew, science party, and PMEL Ocean Climate Stations and Carbon Program group technicians, who made this data set possible. Data are publicly available at the following links for the NOAA Station Papa buoy http://www.pmel.noaa.gov/ocs/, repeat hydrography cruises http://cdiac.ornl.gov/oceans/, and WOA https://www.nodc.noaa.gov/OC5/woa13/. This work was funded by the NOAA Climate Program Office Climate Observation Division, the NOAA Ocean Acidification Program, and the NSF IGERT Program on Ocean Change and is PMEL contribution 4340.

References

Anderson, L. A. L. A., and J. L. Sarmiento (1994), Redfield ratios of remineralization determined by nutrient data analysis, *Global Biogeochem. Cycles*, *8*(1), 65–80, doi:10.1029/93GB03318.

Astor, Y. M., L. Lorenzoni, R. Thunell, R. Varela, F. Muller-Karger, L. Troccoli, G. T. Taylor, M. I. Scranton, E. Tappa, and D. Rueda (2013), Interannual variability in sea surface temperature and fCO_2 changes in the Cariaco Basin, *Deep Sea Res., Part II*, *93*, 33–43, doi:10.1016/j.dsr2.2013.01.002.

Atlas, R., R. N. Hoffman, J. Ardizzone, S. M. Leidner, J. C. Jusem, D. K. Smith, and D. Gombos (2011), A cross-calibrated, multiplatform ocean surface wind velocity product for meteorological and oceanographic applications, *Bull. Am. Meteorol. Soc.*, *92*(2), 157–174, doi:10.1175/2010BAMS2946.1.

Ayers, J. M., and M. S. Lozier (2012), Unraveling dynamical controls on the North Pacific carbon sink, *J. Geophys. Res.*, *117*, C01017, doi:10.1029/2011JC007368.

Bates, N. R. (2012), Multi-decadal uptake of carbon dioxide into subtropical mode water of the North Atlantic Ocean, *Biogeosciences*, *9*(7), 2649–2659, doi:10.5194/bg-9-2649-2012.

Bates, N. R., Y. M. Astor, M. J. Church, K. Currie, J. E. Dore, M. González-Dávila, L. Lorenzoni, F. Muller-Karger, J. Olafsson, and J. M. Santana-Casiano (2014), A time-series view of changing surface ocean chemistry due to ocean uptake of anthropogenic CO_2 and ocean acidification, *Oceanography*, *27*(1), 126–141, doi:10.5670/oceanog.2014.16.

Bentamy, A., and D. C. Fillon (2012), Gridded surface wind fields from Metop/ASCAT measurements, *Int. J. Remote Sens.*, *33*(6), 1729–1754, doi:10.1080/01431161.2011.600348.

Bishop, K. B., S. E. Calvert, and M. Y. S. Soon (1999), Spatial and temporal variability of POC in the northeast subarctic Pacific, *Deep Sea Res., Part II*, *46*(11-12), 2699–2733, doi:10.1016/S0967-0645(99)00081-8.

Bonjean, F., and G. S. E. Lagerloef (2002), Diagnostic model and analysis of the surface currents in the tropical Pacific Ocean, *J. Phys. Oceanogr.*, *32*, 2938–2954.

Brix, H., N. Gruber, and C. C. D. Keeling (2004), Interannual variability of the upper ocean carbon cycle at station ALOHA near Hawaii, *Global Biogeochem. Cycles*, *18*, GB4019, doi:10.1029/2004GB002245.

Carlson, C. A., H. W. Ducklow, and A. F. Michaels (1994), Annual flux of dissolved organic carbon from the euphotic zone in the northwestern Sargasso Sea, *Nature*, *371*(6496), 405–408, doi:10.1038/371405a0.

Charette, M. A., S. Bradley Moran, and J. K. B. Bishop (1999), ^{234}Th as a tracer of particulate organic carbon export in the subarctic northeast Pacific Ocean, *Deep Sea Res., Part II*, *46*(11-12), 2833–2861, doi:10.1016/S0967-0645(99)00085-5.

Chierici, M., A. Fransson, and Y. Nojiri (2006), Biogeochemical processes as drivers of surface fCO_2 in contrasting provinces in the subarctic North Pacific Ocean, *Global Biogeochem. Cycles*, *20*, GB1009, doi:10.1029/2004GB002356.

Ciais, P., et al. (2013), Carbon and other biogeochemical cycles, in *Climate Change 2013: The Physical Science Basis—Contribution of Working Group I to the Fifth Assessment Report of the Intergovernmental Panel on Climate Change*, edited by T. F. Stocker et al., Cambridge Univ. Press, Cambridge, U. K., and New York.

Cronin, M. F., N. A. Bond, J. T. Farrar, H. Ichikawa, S. R. Jayne, Y. Kawai, M. Konda, B. Qiu, L. Rainville, and H. Tomita (2013), Formation and erosion of the seasonal thermocline in the Kuroshio Extension Recirculation Gyre, *Deep Sea Res., Part II*, *85*, 62–74, doi:10.1016/j.dsr2.2012.07.018.

Cronin, M. F., N. A. Pelland, S. R. Emerson, and W. R. Crawford (2015), Estimating diffusivity from the mixed layer heat and salt balances in the North Pacific, *J. Geophys. Res. Ocean*, *120*, 7346–7362, doi:10.1002/2015JC011010.

Cullison Gray, S. E., M. D. DeGrandpre, T. S. Moore, T. R. Martz, G. Friederich, and K. S. Johnson (2011), Applications of in situ pH measurements for inorganic carbon calculations, *Mar. Chem.*, *125*, 82–90, doi:10.1016/j.marchem.2011.02.005.

de Boyer Montégut, C., G. Madec, A. S. Fischer, A. Lazar, and D. Iudicone (2004), Mixed layer depth over the global ocean: An examination of profile data and a profile-based climatology, *J. Geophys. Res.*, *109*, C12003, doi:10.1029/2004JC002378.

Dickson, A. G. (1990), Standard potential of the reaction: AgCl(s) + 1/2H_2(g) = Ag(s) + HCl(aq), and the standard acidity constant of the ion HSO_4^- in synthetic sea water from 273.15 to 318.15 K, *J. Chem. Thermodyn.*, *22*, 113–127.

Dickson, A. G., and J. Riley (1978), The effect of analytical error on the evaluation of the components of the aquatic carbon-dioxide system, *Mar. Chem.*, *6*, 77–85, doi:10.1016/0304-4203(78)90008-7.

Dore, J., R. Lukas, D. W. Sadler, M. J. Church, and D. M. Karl (2009), Physical and biogeochemical modulation of ocean acidification in the central North Pacific, *Proc. Natl. Acad. Sci. U. S. A.*, *106*(30), 12,235–12,240, doi:10.1073/pnas.0906044106.

Emerson, S. (2014), Annual net community production and the biological carbon flux in the ocean, *Global Biogeochem. Cycles*, *28*, 14–28, doi:10.1002/2013GB004680.

Emerson, S., and C. Stump (2010), Net biological oxygen production in the ocean-II: Remote in situ measurements of O_2 and N_2 in subarctic pacific surface waters, *Deep Sea Res., Part I*, *57*(10), 1255–1265, doi:10.1016/j.dsr.2010.06.001.

Emerson, S., C. Sabine, M. F. Cronin, R. Feely, S. E. Cullison Gray, and M. Degrandpre (2011), Quantifying the flux of $CaCO_3$ and organic carbon from the surface ocean using in situ measurements of O_2, N_2, pCO_2, and pH, *Global Biogeochem. Cycles*, *25*, GB3008, doi:10.1029/2010GB003924.

Emerson, S. R. (1987), Seasonal oxygen cycles and biological new production in surface waters of the subarctic Pacific Ocean, *J. Geophys. Res.*, *92*, 6535–6544, doi:10.1029/JC092iC06p06535.

Emerson, S. R., P. D. Quay, C. Stump, D. Wilbur, and M. Knox (1991), O_2, Ar, N_2, and ^{222}Rn in surface waters of the subarctic ocean: Net biological O_2 production, *Global Biogeochem. Cycles*, *5*(1), 49–69, doi:10.1029/90GB02656.

Fassbender, A. J., C. L. Sabine, N. Lawrence-Slavas, E. H. De Carlo, C. Meinig, and S. Maenner Jones (2015), Robust sensor for extended autonomous measurements of surface ocean dissolved inorganic carbon, *Environ. Sci. Technol.*, *49*(6), 3628–3625, doi:10.1021/es5047183.

Feely, R. A., et al. (2002), In situ calcium carbonate dissolution in the Pacific Ocean, *Global Biogeochem. Cycles*, *16*(4), 1144, doi:10.1029/2002GB001866.

Feely, R. A., et al. (2008), Carbon dioxide, hydrographic, and chemical data obtained during the R/Vs *Roger Revelle* and *Thomas G. Thompson* repeat hydrography cruises in the Pacific Ocean: CLIVAR CO_2 sections P16S_2005 and P16N_2006 ORNL/CDIAC-155 NDP-090, Carbon Dioxide Information Analysis Center, Oak Ridge National Laboratory, U. S. Department of Energy, Oak Ridge, Tenn.

Feely, R. A., C. L. Sabine, and S. R. Emerson (2011), Carbon dioxide, hydrographic, and chemical data obtained during the R/V *Thomas Thompson* "Student" Cruise TN224 in the Pacific Ocean (August 26–September 17, 2008) Carbon Dioxide Information Analysis Center, Oak Ridge National Laboratory, U. S. Department of Energy, Oak Ridge, Tenn.

Freeland, H. J. (2007), A short history of Ocean Station Papa and Line P, *Prog. Oceanogr.*, *75*(2), 120–125, doi:10.1016/j.pocean.2007.08.005.

Fukasawa, M., T. Kawano, A. Murata, H. Uchida, and T. Doi (2007), Carbon dioxide, hydrographic, and chemical data obtained during the R/V *Mirai* repeat hydrography cruise in the Pacific Ocean: CLIVAR CO2 section P01 2007 (July 24–September 3, 2007) Carbon Dioxide Information Analysis Center, Oak Ridge National Laboratory, U. S. Department of Energy, Oak Ridge, Tenn.

Garcia, H. E., R. A. Locarnini, T. P. Boyer, J. I. Antonov, O. K. Baranova, M. M. Zweng, J. R. Reagan, and D. R. Johnson (2013a), *World Ocean Atlas 2013, Dissolved Inorganic Nutrients (Phosphate, Nitrate, Silicate)*, *NOAA Atlas NESDIS 76*, vol. 4, edited by S. Levitus and A. Mishonov, U. S. U.S. Gov. Print. Off., Washington, D. C.

Garcia, H. E., R. A. Locarnini, T. P. Boyer, J. I. Antonov, A. V. Mishonov, O. K. Baranova, M. M. Zweng, J. R. Reagan, and D. R. Johnson (2013b), *World Ocean Atlas 2013, Dissolved Oxygen, Apparent Oxygen Utilization, and Oxygen Saturation*, *NOAA Atlas NESDIS 75*, vol. 3, edited by S. Levitus and A. Mishonov, U.S. Gov. Print. Off., Washington, D. C.

Giesbrecht, K. E., R. C. Hamme, and S. R. Emerson (2012), Biological productivity along Line P in the subarctic northeast Pacific: In situ versus incubation-based methods, *Global Biogeochem. Cycles*, *26*, GB3028, doi:10.1029/2012GB004349.

Gledhill, D., R. Wanninkhof, and C. M. Eakin (2009), Observing ocean acidification from space, *Oceanography*, *22*(4), 48–59, doi:10.5670/oceanog.2009.96.

González-Dávila, M., J. M. Santana-Casiano, M. J. Rueda, and O. Llinás (2010), The water column distribution of carbonate system variables at the ESTOC site from 1995 to 2004, *Biogeosciences*, *7*(10), 3067–3081, doi:10.5194/bg-7-3067-2010.

Gruber, N., C. D. Keeling, and T. F. Stocker (1998), Carbon-13 constraints on the seasonal inorganic carbon budget at the BATS site in the northwestern Sargasso Sea, *Deep Sea Res., Part I*, *45*(4-5), 673–717, doi:10.1016/S0967-0637(97)00098-8.

Hales, B., P. G. Strutton, M. Saraceno, R. Letelier, T. Takahashi, R. A. Feely, C. L. Sabine, and F. P. Chavez (2012), Satellite-based prediction of pCO_2 in coastal waters of the eastern North Pacific, *Prog. Oceanogr.*, *103*, doi:10.1016/j.pocean.2012.03.001.

Hamme, R. C., et al. (2010), Volcanic ash fuels anomalous plankton bloom in subarctic northeast Pacific, *Geophys. Res. Lett.*, *37*, L19604, doi:10.1029/2010GL044629.

Hansell, D. (2001), Marine dissolved organic matter and the carbon cycle, *Oceanography*, *14*(4), 41–49, doi:10.5670/oceanog.2001.05.

Ho, D. T., C. S. Law, M. J. Smith, P. Schlosser, M. Harvey, and P. Hill (2006), Measurements of air-sea gas exchange at high wind speeds in the Southern Ocean: Implications for global parameterizations, *Geophys. Res. Lett.*, *33*, L16611, doi:10.1029/2006GL026817.

Jin, X., N. Gruber, J. P. Dunne, J. L. Sarmiento, and R. A. Armstrong (2006), Diagnosing the contribution of phytoplankton functional groups to the production and export of particulate organic carbon, $CaCO_3$, and opal from global nutrient and alkalinity distributions, *Global Biogeochem. Cycles*, *20*, BG2015, doi:10.1029/2005GB002532.

Johnson, K. S., W. M. Berelson, E. S. Boss, Z. Chase, H. Claustre, S. R. Emerson, N. Gruber, A. Kortzinger, M. J. Perry, and S. C. Riser (2009), Observing biogeochemical cycles at global scales with profiling floats and gliders: Prospects for a global array, *Oceanography*, *22*, 216–225.

Juranek, L. W., P. D. Quay, R. A. Feely, D. Lockwood, D. M. Karl, and M. J. Church (2012), Biological production in the NE Pacific and its influence on air-sea CO_2 flux: Evidence from dissolved oxygen isotopes and O_2/Ar, *J. Geophys. Res.*, *117*, C05022, doi:10.1029/2011JC007450.

Keeling, C. D., H. Brix, and N. Gruber (2004), Seasonal and long-term dynamics of the upper ocean carbon cycle at Station ALOHA near Hawaii, *Global Biogeochem. Cycles*, *18*, GB4006, doi:10.1029/2004GB002227.

Körtzinger, A., U. Send, R. S. Lampitt, S. Hartman, D. W. R. Wallace, J. Karstensen, M. G. Villagarcia, O. Llinás, and M. D. DeGrandpre (2008), The seasonal pCO_2 cycle at 49°N/16.5°W in the northeastern Atlantic Ocean and what it tells us about biological productivity, *J. Geophys. Res.*, *113*, C04020, doi:10.1029/2007JC004347.

Lauvset, S. K., N. Gruber, P. Landschützer, A. Olsen, and J. Tjiputra (2015), Trends and drivers in global surface ocean pH over the past 3 decades, *Biogeosciences*, *12*(5), 1285–1298, doi:10.5194/bg-12-1285-2015.

Lipsen, M. S., D. W. Crawford, J. Gower, and P. J. Harrison (2007), Spatial and temporal variability in coccolithophore abundance and production of PIC and POC in the NE subarctic Pacific during El Niño (1998), La Niña (1999) and 2000, *Prog. Oceanogr.*, *75*(2), 304–325, doi:10.1016/j.pocean.2007.08.004.

Liu, W. T., K. B. Katsaros, and J. A. Businger (1979), Bulk parameterization of air-sea exchanges of heat and water vapor including the molecular constraints at the interface, *J. Atmos. Sci.*, *36*(9), 1722–1735.
Locarnini, R. A., et al. (2013), in *World Ocean Atlas 2013, Temperature*, *NOAA Atlas NESDIS 73*, vol. 1, edited by S. Levitus and A. Mishonov, U.S. Gov. Print. Off., Washington, D. C.
Lockwood, D. (2013), Impact of the marine biological pump on atmospheric CO_2 uptake in the North Pacific: A study based on basin-wide underway measurements of oxygen/argon gas ratios and pCO_2, PhD dissertation, Univ. of Washington, Seattle, Washington.
Lomas, M. W., N. R. Bates, R. J. Johnson, A. H. Knap, D. K. Steinberg, and C. A. Carlson (2013), Two decades and counting: 24-years of sustained open ocean biogeochemical measurements in the Sargasso Sea, *Deep Sea Res., Part II*, *93*, 16–32, doi:10.1016/j.dsr2.2013.01.008.
Lueker, T. J., A. G. Dickson, and C. D. Keeling (2000), Ocean pCO_2 calculated from dissolved inorganic carbon, alkalinity, and equations for K_1 and K_2: Validation based on laboratory measurements of CO_2 in gas and seawater at equilibrium, *Mar. Chem.*, *70*, 105–119, doi:10.1016/S0304-4203(00)00022-0.
Martin, J. H., and S. E. Fitzwater (1988), Iron deficiency limits phytoplankton growth in the north-east Pacific subarctic, *Nature*, *331*(6154), 341–343, doi:10.1038/331341a0.
McGillicuddy, D. J., Jr., A. R. Robinson, D. A. Siegel, H. W. Jannasch, R. Johnson, T. D. Dickey, J. McNeil, A. F. Michaels, and A. H. Knap (1998), Influence of mesoscale eddies on new production in the Sargasso Sea, *Nature*, *394*, 263–266, doi:10.1038/28367.
McGillicuddy, D. J., Jr., et al. (2007), Eddy/wind interactions stimulate extraordinary mid-ocean plankton blooms, *Science*, *316*(5827), 1021–1026, doi:10.1126/science.1136256.
Miller, L. A., J. Christian, M. Davelaar, W. K. Johnson, and J. Linguanti (2010), *Carbon Dioxide, Hydrographic and Chemical Data Obtained During the Time Series Line P Cruises in the North-East Pacific Ocean From 1985–2010*, Carbon Dioxide Information Analysis Center, Oak Ridge National Laboratory, U. S. Department of Energy, Oak Ridge, Tenn.
Millero, F. J. (2007), The marine inorganic carbon cycle, *Chem. Rev.*, *107*, 308–341, doi:10.1021/cr0503557.
Passow, U., and C. A. Carlson (2012), The biological pump in a high CO_2 world, *Mar. Ecol. Prog. Ser.*, *470*(2), 249–271, doi:10.3354/meps09985.
Quay, P. D., and J. Stutsman (2003), Surface layer carbon budget for the subtropical N. Pacific: Constraints at station ALOHA, *Deep Sea Res., Part I*, *50*(9), 1045–1061, doi:10.1016/S0967-0637(03)00116-X.
Rhein, M., et al. (2013), Observations: Ocean, in *Climate Change 2013: The Physical Science Basis. Contribution of Working Group I to the Fifth Assessment Report of the Intergovernmental Panel on Climate Change*, edited by T. F. Stocker et al., Cambridge Univ. Press, Cambridge, New York.
Sarmiento, J. L., J. P. Dunne, A. Gnanadesikan, R. M. Key, K. Matsumoto, and R. Slater (2002), A new estimate of the CaCO3 to organic carbon export ratio, *Global Biogeochem. Cycles*, *16*(4), 1107, doi:10.1029/2002GB001919.
Send, U., et al. (2010), OceanSITES, in *Proceedings of OceanObs'09: Sustained Ocean Observations and Information for Society*, vol. 2, edited by J. Hall, D. E. Harrison, and D. Stammer, ESA Publ. WPP-306, Venice, Italy, 21-25 Sept. 2009, doi:10.5270/OceanObs09.cwp.79.
Signorini, S. R., C. R. McClain, J. R. Christian, and C. Wong (2001), Seasonal and interannual variability of phytoplankton, nutrients, TCO_2, pCO_2, and O_2 in the eastern subarctic Pacific (ocean weather station Papa), *J. Geophys. Res.*, *106*(C12), 31,197–31,215, doi:10.1029/2000JC000343.
Sugiura, K., and S. Tsunogai (2005), Spatial and temporal variation of surface xCO_2 providing net biological productivities in the Western North Pacific in June, *J. Oceanogr.*, *61*(3), 435–445, doi:10.1007/s10872-005-0052-0.
Sutton, A. J., et al. (2014), A high-frequency atmospheric and seawater pCO_2 data set from 14 open ocean sites using a moored autonomous system, *Earth Syst. Sci. Data*, *6*, 353–366, doi:10.5194/essdd-7-385-2014.
Takahashi, T., J. G. Goddard, and D. W. Chipman (1993), Seasonal variation of CO_2 and nutrients in the high-latitude surface oceans: A comparative study, *Global Biogeochem. Cycles*, *7*(4), 843–878, doi:10.1029/93GB02263.
Takahashi, T., S. C. Sutherland, R. A. Feely, and R. Wanninkhof (2006), Decadal change of the surface water pCO_2 in the North Pacific: A synthesis of 35 years of observations, *J. Geophys. Res.*, *111*, C07S05, doi:10.1029/2005JC003074.
Takahashi, T., et al. (2009), Climatological mean and decadal change in surface ocean pCO_2, and net sea-air CO_2 flux over the global oceans, *Deep Sea Res., Part II*, *56*(8-10), 554–577, doi:10.1016/j.dsr2.2008.12.009.
Taylor, G. T., et al. (2012), Ecosystem responses in the southern Caribbean Sea to global climate change, *Proc. Natl. Acad. Sci. U. S. A.*, *109*(47), 19,315–19,320, doi:10.1073/pnas.1207514109.
Timothy, D. A., C. S. Wong, J. E. Barwell-Clarke, J. S. Page, L. A. White, and R. W. Macdonald (2013), Climatology of sediment flux and composition in the subarctic northeast pacific ocean with biogeochemical implications, *Prog. Oceanogr.*, *116*, 95–129, doi:10.1016/j.pocean.2013.06.017.
van Heuven, S., D. Pierrot, J. W. B. Rae, E. Lewis, and D. W. R. Wallace (2011), MATLAB Program Developed for CO_2 System Calculations ORNL/CDIAC-105b., *ORNL/CDIAC-105b. Carbon Dioxide Inf. Anal. Center, Oak Ridge Natl. Lab. U.S. Dep. Energy, Oak Ridge, Tennessee*, doi:10.3334/CDIAC/otg.CO2SYS_MATLAB_v1.1.
Wanninkhof, R. (1992), Relationship between wind speed and gas exchange over the ocean, *J. Geophys. Res.*, *97*(C5), 7373–7382, doi:10.1029/92JC00188.
Weiss, R. (1974), Carbon dioxide in water and seawater: The solubility of a non-ideal gas, *Mar. Chem.*, *2*(3), 203–215, doi:10.1016/0304-4203(74)90015-2.
Winn, C. D., Y.-H. H. Li, F. T. MacKenzie, and D. M. Karl (1998), Rising surface ocean dissolved inorganic carbon at the Hawaii Ocean Time-series site, *Mar. Chem.*, *60*(1-2), 33–47, doi:10.1016/S0304-4203(97)00085-6.
Wolf-Gladrow, D., R. E. Zeebe, C. Klaas, A. Kortzinger, and A. G. Dickson (2007), Total alkalinity: The explicit conservative expression and its application to biogeochemical processes, *Mar. Chem.*, *106*(1-2), 287–300, doi:10.1016/j.marchem.2007.01.006.
Wong, C. S., F. A. Whitney, K. Iseki, J. S. C. Page, and J. Zeng (1995), Analysis of trends in primary productivity and chlorophyll-a over two decades at Ocean Station P (50 N, 145 W) in the subarctic Northeast Pacific Ocean, *Can. Spec. Publ. Fish. Aquat. Sci.*, *121*, 107–117.
Wong, C. S., F. A. Whitney, D. W. Crawford, K. Iseki, R. J. Matear, W. K. Johnson, J. S. Page, and D. Timothy (1999), Seasonal and interannual variability in particle fluxes of carbon, nitrogen and silicon from time series of sediment traps at Ocean Station P, 1982-1993: Relationship to changes in subarctic primary productivity, *Deep. Res. Part II*, *46*(11-12), 2735–2760, doi:10.1016/S0967-0645(99)00082-X.
Wong, C. S., N. A. D. Waser, Y. Nojiri, W. K. Johnson, F. A. Whitney, J. S. C. Page, and J. Zeng (2002a), Seasonal and interannual variability in the distribution of surface nutrients and dissolved inorganic carbon in the northern North Pacific: Influence of El Niño, *J. Oceanogr.*, *58*(2), 227–243.
Wong, C. S., N. A. D. Waser, Y. Nojiri, F. A. Whitney, J. S. Page, and J. Zeng (2002b), Seasonal cycles of nutrients and dissolved inorganic carbon at high and mid latitudes in the North Pacific Ocean during the Skaugran cruises: Determination of new production and nutrient uptake ratios, *Deep Sea Res., Part II*, *49*(24-25), 5317–5338, doi:10.1016/S0967-0645(02)00193-5.
Wong, C. S., N. A. D. Waser, F. A. Whitney, W. K. Johnson, and J. S. Page (2002c), Time-series study of the biogeochemistry of the North East subarctic Pacific: Reconciliation of the Corg/N remineralization and uptake ratios with the Redfield ratios, *Deep Sea Res., Part II*, *49*(24-25), 5717–5738, doi:10.1016/S0967-0645(02)00211-4.
Zweng, M. M., et al. (2013), in *World Ocean Atlas 2013, Salinity*, vol. 2, edited by S. Levitus and A. Mishonov, U. S. Government Printing Office, Washington, D. C.